Heterostructures of pseudomorphic $Ge_{1-y}C_y$ and $Ge_{1-x-y}Si_xC_y$ alloys grown on Ge (001) substrates

M. W. Dashiell[a] and J. Kolodzey[b]
Department of Electrical and Computer Engineering, University of Delaware, Newark, Delaware 19716

P. Boucaud, Vy Yam, and J.-M. Lourtioz
Institute d'Electronique Fondamental, Universite Paris XI, Batiment 220, 91405 Orsay, France

(Received 10 October 1999; accepted 10 January 2000)

Heterostructures of $Ge_{1-y}C_y$ and $Ge_{1-x-y}Si_xC_y$ on Ge (001) substrates with ($0<y<0.001$) and ($0<x<0.05$) were grown by low temperature molecular beam epitaxy ($T_{growth}=275\,°C$). These carbon fractions exceed by nearly ten orders of magnitude the solid solubility of C in bulk germanium. High resolution x-ray diffraction reveals that the layers are pseudomorphic and have high crystalline quality and interface abruptness, evident from strong Pendellösung fringes and superlattice satellite peaks. The heterostructures are metastable due to the supersaturation of substitutional C in the lattice and the strained layers relax at high temperatures. From x-ray diffraction measurements, we conclude that the relaxation mechanism is due to the loss of C from substitutional sites, rather than by the formation of extended defects. We empirically determined the activation energies for the decrease of substitutional C in pseudomorphic $Ge_{0.999}C_{0.001}$ and $Ge_{0.972}Si_{0.027}C_{0.0008}$ alloys to be 3.4 and 3.6 eV, respectively. Near band-edge photoluminescence is observed from pseudomorphic $Ge_{1-y}C_y$ samples.
[S0734-211X(00)00103-7]

In the past ten years, alloys of SiGeC have been extensively studied in order to exploit strain compensation and band-gap engineering for heterostructure Si technology.[1–3] Germanium rich alloys hold promise for greater band offsets for SiGe/Si heterostructures. Due to the lattice mismatch to Si substrates, however, the layers quickly relax by the generation of extended defects. The addition of the smaller C atom will relieve some of the lattice mismatch on Si substrates, however incorporation of substitutional C becomes increasingly difficult with higher Ge concentrations due to its low solid solubility [$<1\times10^{10}\,cm^{-3}$ (Ref. 4)]. Several groups have studied Ge rich GeSiC alloys, but most have been on Si substrates where the layers are relaxed.[5–7] Only recently has the binary $Ge_{1-y}C_y$ alloy been synthesized on Ge by solid phase epitaxy[8] and by MBE.[9,10] Studying the Ge rich ternary system on a Ge substrate allows the intrinsic alloy properties to be investigated without the presence of defects associated with strain relaxation. In this article, we discuss the properties of the as-grown alloys as well as their thermal stability.

Ternary $Ge_{1-x-y}Si_xC_y$ and binary $Ge_{1-y}C_y$ alloys were grown pseudomorphically on Ge (001) substrates at a nominal growth temperature of 275 °C in an EPI620 MBE system. Carbon was evaporated from a resistively heated pyrolytic graphite filament (MBE-Komponenten, Model SUKO-63). Silicon and Ge were evaporated from a high temperature and standard effusion cell, respectively. The Ge substrates were prepared by degreasing in TCE, acetone, and methanol, etching in dilute hydroflouric acid H_2O:HF(10:1) followed by a final dip in a solution of H_2O and H_2O_2(10:1). The samples were loaded into the MBE chamber and heated to 600 °C to desorb the surface oxide. A 100 nm Ge buffer was grown at 400 °C, followed by the alloy layer at 275 °C and a pure Ge cap layer at 400 °C. The alloy composition and thickness were determined using a Phillip's X'Pert MRD high-resolution x-ray diffractometer (HRXRD) and dynamical x-ray simulations. So that the Si content could be independently determined, a reference $Ge_{1-x}Si_x$ binary alloy was grown under identical conditions to the ternary alloy, with the exception of the C shutter being closed.

Table I lists the alloy compositions for various Ge growth rates, Si cell temperatures, and C filament currents grown at a constant substrate temperature. The C compositions given are the substitutional (C_{sub}) values determined by HRXRD; the total C concentration might be larger. Figure 1 shows the symmetric (004) x-ray reflections of different binary and ternary $Ge_{1-x-y}Si_xC_y$ compositions. These layers were grown at a rate of 0.25 Å/s, were 420 nm thick, and capped with 70 nm Ge. The x-ray spectra have the angle rescaled so that the Bragg angle of the Ge substrate and buffer is located at 0°. The alloy Bragg peaks are shifted to higher angles relative to the pure Ge substrate, indicating tensile strain, which is expected due to the substitutional incorporation of the smaller Si and C atoms. Also evident are strong Pendellösung fringes, which indicate high crystalline and interface quality.

An important point to note in Table I is that by decreasing the Ge growth rate from 0.6 to 0.01 Å/s, while keeping the C-flux constant ($I_{filament}=92.5$), we did not observe changes in C_{sub} to the extent expected from the change in the Ge to C flux ratio. As the growth rate is decreased from 0.6 to 0.06 Å/s, C_{sub} increases by less than a factor of 2. At a growth rate of 0.01 Å/s, C_{sub} becomes negligible which was evident from the lack of observable alloy strain in the x-ray spectra.

[a]Electronic mail: dashiell@ee.udel.edu
[b]Electronic mail: kolodzey@ee.udel.edu

TABLE I. Table of growth conditions and alloy compositions. All samples listed were grown at 275 °C. The Si and substitutional C concentrations were determined by high resolution x-ray diffraction and dynamical simulations.

Ge growth rate (Å/s)	C cell current (A)	Si cell temperature (°C)	Substitutional C fraction	Si fraction	Alloy thickness (nm)
0.25	90	···	0.0005	···	100
0.25	92.5	···	0.0008	···	420
0.25	94.5	···	0.001	···	420
0.60	92.5	···	0.0008	···	120
0.06	92.5	···	0.0015	···	120
0.01	92.5	···	~0	···	120
0.25	92.5	1375	0.0008	0.027	460
0.25	92.5	1400	0.0008	0.040	460

This is exactly the behavior observed experimentally by Osten *et al.*[11] for the growth of $Si_{1-y}C_y$ on Si (001) and discussed theoretically by Tersoff.[12] The growth requirements for high substitutional C incorporation in Si required that growth rate is high enough to bury the C in its substitutional position before it has time to diffuse to an interstitial site near the surface. Our observations of C_{sub} incorporation as a function of growth rate offers support for the validity of the model discussed above to describe the growth of $Ge_{1-y}C_y$ alloys on the Ge (001) surface.

We measured the differential midinfrared (400–4000 cm^{-1}) absorption of the alloy films using both a Ge substrate and an epitaxial Ge layer grown on a Ge substrate as references. For the binary alloy, we observed only a weak local vibrational mode of C_{sub}(*C*-LVM) in Ge at 529 cm^{-1}.[8] No IR peaks were detected in our pure Ge epitaxial film, so this feature is attributed to *C*. As Si was added, we did not resolve the *C*-LVM in the ternary alloy by IR absorption. This may be due to splitting and broadening of the *C*-LVM due to the different first and second nearest neighbor bonding configurations of C–Ge and C–Si bonds as discussed in Kulik *et al.*,[13] making the peak(s) more difficult to resolve. The presence of substitutional carbon in the ternary alloy, however, is supported by the additional tensile strain observed in the XRD spectra compared to the binary GeSi alloy with equivalent Ge to Si ratio (see Fig. 1).

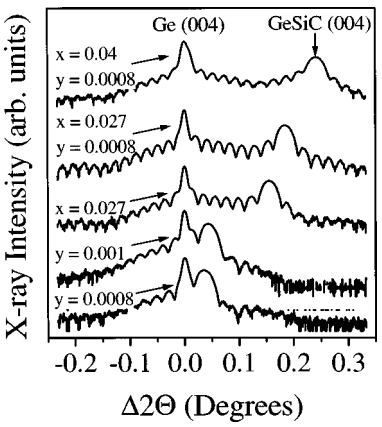

FIG. 1. Symmetric (004) x-ray diffraction reflections of $Ge_{1-x-y}Si_xC_y$ alloys grown pseudomorphically on Ge (001) substrates. These alloy layers are 420 nm thick with a 70 nm Ge cap.

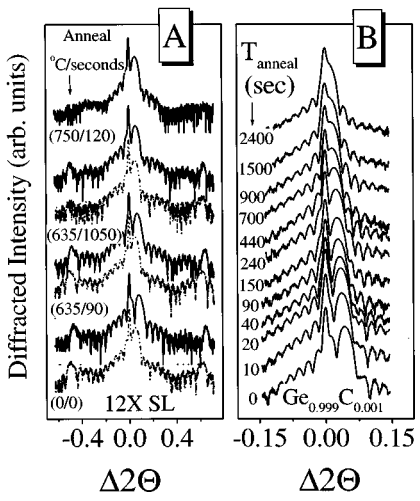

FIG. 2. (A) Symmetric (004) x-ray diffraction reflections vs Bragg angle shift of a 12 (9 nm/10 nm) period $Ge_{0.972}Si_{0.027}C_{0.0008}$/Ge superlattice (SL) (solid line) and the equivalent superlattice structure with no carbon (dotted line). All growth conditions were the same between the two samples with the exception of the C beam being blocked during growth of the latter SL. After selected annealing conditions (indicated in figure) strain conditions in the ternary layer relax to that of the more stable binary alloy SL. (B) Symmetric (004) x-ray diffraction reflections of the pseudomorphic $Ge_{0.999}C_{0.001}$ alloy on Ge (001) after successive 635 °C isothermal anneals (times are indicated in the figure). A decrease in layer strain is observed with increasing time due to loss of substitutional C.

Figure 2(A) displays the symmetric (004) x-ray reflections of a 12 period $Ge_{0.972}Si_{0.027}C_{0.0008}$(9 nm)/Ge(10 mm) superlattice (solid line) and the equivalent superlattice (SL) structure with no carbon (dashed line) for several annealing conditions. Both structures exhibit strong Pendellösung fringes as well as first order SL satellite peaks indicating high crystalline and interface quality. The bottom pair of curves is the x-ray spectra for the as-grown SL samples. There is a clear shift in the zero order SL peak of the ternary alloy towards higher Bragg angles compared to the binary SL sample. This is attributed to the incorporation of the smaller C atom in substitutional sites which increases the average tensile strain compared to the GeSi/Ge SL reference. Because the alloy is metastable, the alloy is expected to relax to its equilibrium state with high temperature annealing. The next two pairs of curves are the x-ray spectra of the ternary and binary SL structure after annealing at 635 °C for 90 and 1050 s. No significant change is observed in the GeSi/Ge SL x-ray spectra over the annealing duration. The zero order peak of the ternary GeSiC SL, however, decreases to lower angles with annealing at 635 °C and approaches the equivalent angular position of the zero-order peak of the GeSi SL as annealing time is increased. At an annealing temperature of 750 °C for 120 s (top curve-solid line), the position of the zero-order peak of the GeSiC/Ge SL is indistinguishable from that of the unannealed GeSi/Ge SL, showing that the average strain of the ternary alloy has relaxed to the equivalent strain condition of the GeSi reference SL. We attribute

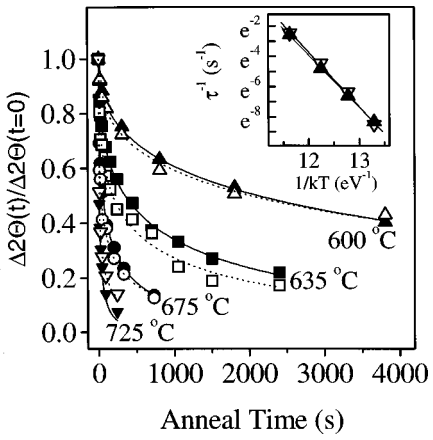

FIG. 3. Plot of the C_{sub} as a function of annealing time normalized to its initial value for pseudomorphic $Ge_{0.972}Si_{0.027}C_{0.0008}$ (open symbols) and $Ge_{0.999}C_{0.001}$ (closed symbols) alloys. The inset shows the Arrhenius plot of the decay constant, τ^{-1} vs $1/k_BT$ where k_B is Boltzmann's constant and T is the annealing temperature. An activation energy of 3.4 and 3.6 eV was obtained for $Ge_{0.999}C_{0.001}$ and $Ge_{0.972}Si_{0.027}C_{0.0008}$, respectively.

the decrease in strain with annealing to the ejection of C from substitutional lattice sites. We rule out the formation of extended defects in the ternary layer, since the strong Pendellösung fringes remain after annealing. For the 750 °C anneal, the disappearance of the satellite superlattice peaks suggests that the interface sharpness has degraded, probably due to Ge–Si interdiffusion.

To quantify the thermal stability of the alloys, we have studied the systematic change in average lattice constant of the pseudomorphic alloy layers with annealing. Annealing was performed in forming gas in a Heatpulse rapid thermal annealing (RTA) furnace for temperatures between 600 and 725 °C. Figure 2(B) shows the symmetric (004) x-ray reflection of the 420 nm thick $Ge_{0.999}C_{0.001}$ alloy after successive isothermal anneals at 635 °C. Similar to the case of the GeSiC SL, the average tensile strain decreases towards the case of zero substitutional carbon. Infrared absorption show that the *C*-LVM intensity in the binary alloy is decreasing with high temperature anneals, which supports the interpretation that the decrease in strain is due to the ejection of C from substitutional sites. The experiments were duplicated for the $GeSi_{0.027}C_{0.0008}$ alloys and performed at temperatures of 600, 635, 675, and 725 °C.

Figure 3 plots the difference of the alloy layer Bragg angle relative to that of pure Ge$[\Delta 2\Theta(t)]$ normalized to its initial value $[(\Delta 2\Theta(t=0))]$ against the annealing time for the two alloys discussed above and at four different annealing temperatures. We have assumed that the decrease in substitutional C concentration is linearly proportional to the decrease in the relative spacing between the Bragg angle of the alloy and that of Ge (Vegard's law). The curves were fitted to the empirical expression given in Ref. 10 describing the loss of C_{sub} in $Ge_{1-y}C_y$ alloys:

$$\frac{\Delta 2\Theta(t)}{\Delta 2\Theta(t=0)} = \frac{C_{sub}(t)}{C_{sub}(t=0)} = \exp\left\{-\left(\frac{t}{\tau}\right)^n\right\}, \quad (1)$$

where τ is a decay constant and n characterizes the process involved in precipitate formation. We obtained values of n about 0.4 for all temperatures and for both compositions, in agreement with Ref. 10 for GeC superlattices. The inset of Fig. 3 displays the Arrhenius plot of τ^{-1} vs $1/k_BT_{anneal}$ where k_B is the Boltzmann constant. The value of τ^{-1} may be interpreted as a thermally activated rate for the loss of substitutional C, where $\tau^{-1} \sim \exp[-E_A/k_BT]$. We obtain $E_A = 3.4 \pm 0.15$ eV and 3.6 ± 0.2 eV in the pseudomorphic $Ge_{0.999}C_{0.001}$ and the $GeSi_{0.027}C_{0.0008}$ alloys, respectively.

Our value of E_A for pseudomorphic $Ge_{0.999}C_{0.001}$ on Ge is greater than the 2.6 eV obtained by Duschl *et al.*[10] by fitting Eq. (1) to two alloy compositions with higher C_{sub} fractions ($y=0.005$ and $y=0.008$) than ours. Our previous results[14] for Si rich SiGeC alloys on Si indicate that the activation energy characterizing the loss of substitutional carbon is dependent on two contributions: (i) the microscopic strain around the C atom due to the atomic mismatch between it and the larger Si and Ge atoms and (ii) the total strain energy of the strained alloy layer grown on a substrate of different lattice constant. For the former contribution, the activation energy will decrease monotonically as the microscopic strain energy around the individual C atom increases. For the latter case, the contribution to E_A will depend on the magnitude of the alloy layer's total strain energy prior to and after the ejection of C from its substitutional sites, so that this contribution to the activation energy is negative if the ejection of C_{sub} decreases the total elastic strain energy in the layer. Our larger activation energy for $Ge_{0.999}C_{0.001}$ compared to the value of E_A measured in Ref. 10 for pseudomorphic $Ge_{0.995}C_{0.005}$ and $Ge_{0.992}C_{0.008}$ alloys suggests a compositional dependence of the activation energy, possibly related to total strain energy of the alloy layer. Other possible contributions to the differences in activation energies could be related to defects generated during growth, since the diffusion and ejection of C_{sub} will most likely involve reactions with point defects such as vacancies and interstitial C atoms or complexes. It is not yet clear how the relative concentrations of these defects affects the thermal stability of the alloys.

Our activation energy is greater than what would qualitatively be predicted by extrapolating to high Ge fractions the activation energies obtained in Si rich SiGeC alloys.[14] For samples with large Si content, the mechanism for relaxation is SiC precipitation, which clearly cannot occur in $Ge_{1-y}C_y$ alloys. Thus the mechanism for relaxation in $Ge_{1-y}C_y$ alloys must differ, and the difference between our obtained E_A and that obtained from extrapolating from the Si-rich SiGeC alloy system is not surprising. Recently, graphitic C phases in annealed $Ge_{1-y}C_y$ on Si(001) samples with $y<0.07$ have been observed with Raman spectroscopy,[6] suggesting that C_{sub} may diffuse to form graphite precipitates.

To further qualify the material quality of these alloys we performed photoluminescence (PL) experiments on selected alloy samples. PL was detected from three different structures at 2.8 K under excitation from an Ar laser. The dotted line in Fig. 4 shows the PL spectrum of the epitaxial Ge

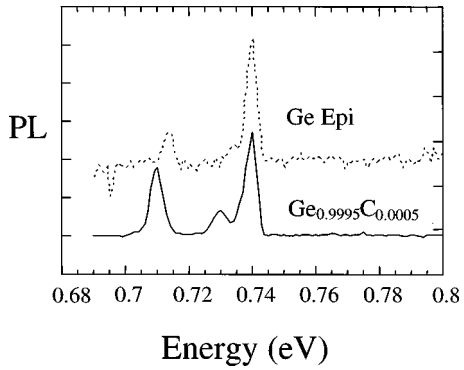

FIG. 4. Photoluminescence spectra of epitaxial Ge (dotted line) and pseudomorphic $Ge_{0.9995}C_{0.0005}$ on Ge (solid line). The high energy peak at 740 meV is assigned to the NP recombination line of Ge. The alloy layer exhibits TA and LA assisted peaks at 730 and 710 meV, respectively, that are shifted by 5 meV with respect to the pure Ge reference sample.

measured with an excitation density of 7 W/cm^2. Luminescence peaks are observed at 740 and 714 meV. Based on results published for pure Ge,[15,16] these are tentatively assigned to a no-phonon (NP) exciton peak and a longitudinal acoustic (LA) phonon replica, respectively. A slight peak is observed at 735 meV, which may be the transverse acoustic (TA) phonon replica of the free exciton. These lines correspond to the same positions (but not the intensity ratios) measured for a commercially available intrinsic Ge substrate measured under equivalent conditions (not shown). A possible explanation for the relative strength of the NP peak in our Ge layer may be a lattice disorder due to the low temperature growth, which may produce point defects. The solid line in Fig. 4 displays the PL spectra of 100 nm thick $Ge_{0.9995}C_{0.0005}$ alloy with a 40 nm thick Ge cap measured under 4 W/cm^2 excitation. Three luminescence peaks are observed at 740, 730, and 709 meV, which possibly are the NP, the TA and the LA recombination lines, respectively. Compared to the pure Ge sample, the phonon replicas have redshifted by $\sim$5 meV. Weak PL was observed in $Ge_{0.9985}C_{0.0015}$ (not shown) with identical shifts of the phonon replica relative to the epitaxial Ge reference.

An explanation for the phonon shift with the addition of carbon is difficult since a systematic study at variable temperatures and excitations is not available at this time. It is interesting to note, however, that the redshift of the phonon replicas with C, did not shift with additional C_{sub} up to $y = 0.0015$. The 5 meV shift is the same energy that several authors have attributed to the energy lowering due to formation of an electron-hole droplet (EHD).[15–17] The positions of the LA and TA phonon peaks in the $Ge_{0.9995}C_{0.0005}$ sample are identical in position to that observed in Fig. 4 of Ref. 16 for the luminescence spectra of the EHD in Ge. Our Ge layer exhibits the spectral characteristic of free-exciton recombination even under higher excitation density (higher carrier density), where EHD formation would be more favorable. It may be speculated that the alloy layer may introduce a potential fluctuation (be it localized around C or at the heterostructure potential well), which increases the exciton density near the fluctuation, resulting in the formation of the EHD. The shift of the phonon replicas with the addition of C suggests that the phonon-assisted luminescence is originating from the alloy layer. It is not clear if the NP luminescent peak of the alloy has shifted with the addition of C. A low energy shoulder was observed on the 740 meV peak of the alloy sample, but its energy could not be resolved.

In conclusion, we have synthesized pseudomorphic, metastable $Ge_{1-y}C_y$ and $Ge_{1-x-y}Si_xC_y$ alloys and superlattices on Ge (001) substrates, which exhibit high crystalline and interface quality. The C_{sub} incorporation mechanism appears to be thermally activated surface diffusion similar to the incorporation of C in $Si_{1-y}C_y$ alloys on Si(001). We present evidence of photoluminescence from the binary $Ge_{1-y}C_y$ alloy, an important result for optoelectronic studies. For our composition range, the binary and ternary alloys are metastable, relaxing by the ejection of C from substitutional sites. This process appears to occur at a rate greater than that of Ge–Si interdiffusion. The activation energy describing the rate of loss of substitutional C in pseudomorphic $Ge_{0.999}C_{0.001}$ and $GeSi_{0.027}C_{0.0008}$ alloys is 3.4 and 3.6 eV, respectively. This implies that the alloys will be stable for processing temperatures of less than 550 °C.

The authors acknowledge support for this research by the ARO under Grant Nos. DAAH04-95-1-0625 and AASERT DAAG55-97-1-0249, and by the ONR under Grant No. N00014-93-1-0393. The authors thank Dr. C. Guedj for assistance in the dynamical x-ray simulation. They also acknowledge Dr. K. Eberl, R. Duschl, Dr. L. V. Kulik, and K. Roe for helpful discussions.

[1]H. J. Osten, E. Bugiel, and P. Zaumseil, Appl. Phys. Lett. **64**, 3440 (1994).
[2]R. A. Soref, Proc. IEEE **81**, 1687 (1993).
[3]O. G. Schmidt and K. Eberl, Phys. Rev. Lett. **80**, 3396 (1998).
[4]R. I. Scace and G. A. Slack, J. Chem. Phys. **30**, 1551 (1959).
[5]J. Kolodzey, P. R. Berger, B. A. Orner, D. Hits, F. Chen, A. Khan, X. Shao, M. M. Waite, S. Ismat Shah, C. P. Swann, and K. Unruh, J. Cryst. Growth **157**, 386 (1996).
[6]B.-K. Yang, M. Krishnamurthy, and W. H. Weber, J. Appl. Phys. **82**, 3287 (1997).
[7]B.-K. Yang, M. Krishnamurthy, and W. H. Weber, J. Appl. Phys. **84**, 2011 (1998).
[8]L. Hoffman, J. C. Bach, B. Lech Nielson, P. Leary, R. Jones, and S. Oberg, Phys. Rev. B **55**, 11167 (1997).
[9]W. H. Weber, B.-K. Yang, and M. Krishnamurthy, Appl. Phys. Lett. **73**, 626 (1998).
[10]R. Duschl, O. G. Schmidt, W. Winter, K. Eberl, M. W. Dashiell, J. Kolodzey, N. Y. Jin-Phillipp, and F. Phillipp, Appl. Phys. Lett. **74**, 1150 (1999).
[11]H. J. Osten, M. Kim, K. Pressel, and P. Zaumseil, J. Appl. Phys. **80**, 6711 (1996).
[12]J. Tersoff, Phys. Rev. Lett. **74**, 5080 (1995).
[13]L. V. Kulik, C. Guedj, M. W. Dashiell, J. Kolodzey, and A. Hairie, Phys. Rev. B **59**, 15753 (1999).
[14]L. V. Kulik, D. A. Hits, M. W. Dashiell, and J. Kolodzey, Appl. Phys. Lett. **72**, 1972 (1998).
[15]C. Benoit à la Guillaume, F. Salvan, and M. Voos, J. Lumin. **1–2**, 315 (1970).
[16]C. Benoit à la Guillaume and M. Voos, Phys. Rev. B **5**, 3079 (1972).
[17]C. Benoit à la Guillaume and M. Voos, Phys. Rev. B **10**, 4995 (1974).